Coordination complexes of methimazole with copper: Controlling redox reactions and sulfur extrusion

Jaime M. Murphy,[a,b] Andrea A. E. Gaertner,[a] Amanda Owen,[a] Samantha Struder,[a] Colin D. McMillen,[a] Modi Wetzler,[a] and Julia L. Brumaghim[a,*]

[a]Department of Chemistry, Clemson University, Clemson, SC 29634-0973, USA

[b]Chemistry and Biochemistry Department, Harding University, Searcy, AR 72149, USA

Abstract

Sulfur-containing imidazole thiones are of interest for their redox chemistry and tendency to form disulfide bonds reminiscent of biologically active disulfides. Treating copper(II) with redox-active methimazole in the presence of oxygen results in concomitant copper reduction and formation methimazole disulfide, and ultimately, extrusion of one of the sulfur atoms. Reaction conditions, including stoichiometry, presence of oxygen, and redox state of the metal ion, were varied to examine the mechanistic details that lead to the sulfur extrusion. Six unique products are reported: $[Cu(\kappa^{N,N}\text{-}MMI^{MS})_2(H_2O)_2](HSO_4)_2$, $[Cu(\kappa^{N,N}\text{-}MMI^{MS})_2(H_2O)][CH_3SO_4][HSO_4][H_2O]$, Synthesis of $[Cu(\kappa^{N,N}\text{-}MMI^{MS})_2(H_2O)](CH_3SO_4)_2$, $[Cu(\kappa^{N,N}\text{-}MMI^{MS})(\kappa^{O,O}\text{-}SO_4)(CH_3OH)]$, $[Cu(\kappa^{N,N}\text{-}MMI^{MS})(\kappa^{O,O}\text{-}SO_4)(DMSO)]\cdot 0.5$ DMSO, and $[Cu(\mu,\kappa^{O,O,O}\text{-}SO_4)(\kappa^{N,N}\text{-}MMI^{MS})]_n[CH_3CN]$ (MMI^{MS} = bis(1-methylimidazol-2-yl)sulfide). In all structures, the HSO_4^- and $CH_3SO_4^-$ counterions are generated *in situ.* EPR analysis of the reaction as it proceeds indicates initial formation of a four-coordinate Cu^{2+}-S complex initially that shifts to square planar or octahedral Cu^{2+}-N coordination over the course of the reaction. Formation of the thiyl radical is also observed by EPR analysis using DMPO as a spin trap. Together, these results establish a complete mechanism for sulfur extrusion that proceeds through copper-methimazole binding and redox, superoxide formation, and nucleophilic attack of water or methanol on sulfur, and subsequent nucleophilic aromatic substitution to yield the sulfur-extruded product. Understanding this mechanism lays the foundation for catalyst development for desulfurization and sulfur-containing polymerization reactions.

Keywords

copper; methimazole; sulfur extrusion; heterocyclic thiones; methylsulfate

1. Introduction

Immense diversity in stoichiometry and redox activity has been demonstrated for the coordination of *N*-heterocyclic thioamides with softer metal centers such as Cu^{+} and Fe^{2+} [1-4]. This remarkable flexibility in redox activity has led to the exploration of thioamides in catalysis [5,6], radiopharmaceuticals [7], energy production [8], corrosion resistance [9,10], sensors [11], and organometallic and coordination chemistry [12,13]. Although thioether- and thiol-containing amino acids have attracted considerable attention as ligands due to their bioavailability, imidazole thiones are of recent interest due to their sigma donor bonding ability [4,14], potential for multidentate binding, and redox activity[15]. Methimazole (MMI), is the most widely prescribed hyperthyroid treatment in the U.S. [16]. and is believed to bind Fe^{2+} in the heme protein, thyroid peroxidase [17]. The exact mechanism of action for MMI is poorly understood, and its biological redox activity and metal coordination has not been investigated fully. MMI is also structurally similar to ergothioneine, a known biological antioxidant [18]. Upon oxidation, MMI forms the corresponding disulfide, MMI^{DS}, a reaction reminiscent of cysteine oxidation to cystine.

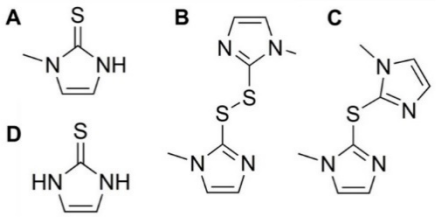

Figure 1. *N*-heterocyclic thione and imidazole disulfide compounds discussed in this study: A) methimazole (MMI), B) methimazole disulfide (MMI^{DS}), C) methimazole monosulfide (MMI^{MS}), and D) 2-mercaptoimidazole (HMI).

Under inert atmosphere conditions, Cu^{+}-MMI coordination has been widely studied, and a wide variety of mono- [19,20], di- [21-24], tetra- [25], and polynuclear [26,27] complexes are reported. With the exception of the two mononuclear Cu^{+} complexes $[Cu(MMI)_3][NO_3]$ [19] and

[Cu(MMI$_3$)Cl] [21], many of the multinuclear and polymeric complexes include *S*-bridging methimazole ligands bound to Cu^+ in trigonal planar or tetrahedral geometry. The dinuclear species can form Cu_2S_2 rhombohedral cores, distorting the tetrahedral coordination around Cu^+. The relatively short Cu-S bond lengths (2.3-2.5 Å) in these dinuclear complexes are similar to the Cu-S(Cys) bond lengths observed in blue copper proteins, and indicate high π-covalency [28].

In an unusual reaction illustrating the facile redox chemistry of methimazole and copper, copper promotes sulfur extrusion from methimazole disulfide (MMI^{DS}) to form a methimazole monosulfide ligand (MMI^{MS}; Figure 1). In the first step, Cu^{2+} oxidizes methimazole to its disulfide and is reduced to Cu^+ (Scheme 1) [15]. In the presence of O_2 from air, Lobana and coworkers [29] proved that Cu^+ was oxidized to Cu^{2+} and the disulfide was oxidized to a sulfone, resulting in sulfur elimination (Scheme 1) and concomitant formation of MMI^{MS}. The *in-situ*-generated MMI^{MS} ligand then coordinates Cu^{2+} in a bidentate fashion through the N atoms on each of the heterocycles [27,29-34]. However, in this proposed mechanism, the role of copper in the mechanistic action of sulfur extrusion, redox activity of the coordinating ion, and stoichiometry of sulfur oxidation were not clearly explained.

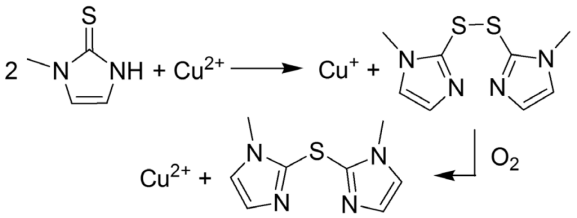

Scheme 1. Reduction of Cu^{2+} by methimazole and subsequent oxidation of Cu^+ with sulfur extrusion in air.

To determine the effects of oxygen and solvent conditions on the coordination chemistry of copper and methimazole and to fully establish the mechanism for sulfur extrusion, a series of reactions Cu^{2+} and Cu^+ with MMI were performed air-free and in air, resulting in several novel dinuclear and polynuclear Cu^+-MMI complexes. Under aerobic conditions, a series of novel Cu^{2+}

complexes with the sulfur-extruded MMI^{MS} ligand were obtained, and EPR studies were performed to obtain a greater mechanistic understanding of this unusual reaction. Fully elucidating this mechanism will provide insight into desulfurization reactions as well as development of syntheses for sulfur-containing polymers.

2. Experimental Methods

2.1. General Methods

2-Mercapto-1-methylimidazole (methimazole), copper(II) nitrate heptahydrate, and copper(II) tetrafluoroborate were purchased commercially. Tetrakis(acetonitrile)copper(I) tetrafluoroborate was prepared according to published procedures [35]. Reactions were performed air-free where indicated, utilizing standard Schlenk techniques under argon. IR spectra of the ligands and complexes were acquired in the range 4000-450 cm^{-1} as Nujol mulls on KBr plates or as KBr pressed pellets, as indicated, on a Magna 550 IR spectrometer or on a Shimazu MIRacle 10 ATR with 100 scans in the range 4000-400 cm^{-1}. IR absorption abbreviations are vs, very strong; s, strong; m, medium; w, weak; b, broad; sh, shoulder. ^{1}H and $^{13}C\{^{1}H\}$ NMR spectra were obtained using Bruker-AVANCE 300 and 500 MHz NMR spectrometers. Chemical shifts are reported in δ relative to tetramethylsilane (δ 0) and referenced to solvent.

MALDI mass spectrometry experiments were performed using a Bruker Microflex MALDI-TOF mass spectrometer with *trans*-2-3-(4-tert-butylphenyl)-2-methyl-2-propenyldiene (*m*/*z* 250.3) as the matrix. Electrospray ionization mass spectrometry (ESI-MS) studies were performed on a Thermo Scientific (San Jose, CA) TSQ QuantumAccess MAX triple quadrupole mass spectrometer. Sample solutions were prepared in 50/50 mixture by volume of H_2O/acetonitrile, and samples were introduced to the ESI source by direct infusion. A scan

containing 5 micro scans was taken every 0.5 s across a 180 to 1000 Da range. For each sample, 100 scans were collected and averaged to obtain a final spectrum. TSQ Tunesoftware (ThermoScientific) was used for data acquisition. ESI-MS data are shown in Figures S2-S8, and both mass/charge ratios and isotopic distributions match simulated envelope intensities. All peak envelopes matched calculated values.

2.2. Synthesis of $[Cu^{I}_2(\mu,\kappa^{S}\text{-MMI})_2(\kappa^{S}\text{-MMI})_4][BF_4]_2$ ***(1)***

Reported complex **1** [23] was synthesized using alternate methods as described.

Method 1. Under air-free conditions, a solution of methimazole (MMI; 137 mg, 1.20 mmol) in acetonitrile (10 mL) was transferred *via* cannula to a solution of $Cu(BF_4)_2{\cdot}6H_2O$ (104 mg, 0.30 mmol) in acetonitrile (5 mL). As MMI was added, a light-green precipitate formed that turned yellow-white upon filtration and drying *in vacuo*. The precipitate was washed with diethyl ether (10 mL). Crystals of **1** were obtained by ether diffusion into an acetonitrile solution. Yield: 566 mg, 57%. IR (Nujol mull, cm^{-1}): 3161 w, 3116 w, 2727 s, 1577 vs, 1517 w, 1462 vs, 1401 vs, 1350 s, 1289 s, 1279 s, 1267 s, 1246 w, 1160 s, 1108 b, 1063 b, 992 b, 918 w, 850 w, 763 s, 728 vs, 695 w, 673 s, 599 w, 515 s. ^{1}H NMR (500 MHz, CD_3CN): δ 3.54 (s, 18H, CH_3), 6.83 and 6.90, (each, d, 6H, C-H, J = 35 Hz), 10.32 (br s, 5.5 H, N-H). $^{13}C\{^{1}H\}$ NMR (CD_3CN): 34.1 (CH_3), 115.1 (CH), 120.9 (CH), 156.5 (C=S).. Anal. Calc. for $C_{24}H_{36}B_2Cu_2F_8N_{12}S_6$: C, 29.24; H, 3.68; N, 17.05. Found: C, 29.03; H, 3.66; N, 16.86.

Method 2. Complex **1** was also synthesized using the procedure described in method 1, except that $[Cu(CH_3CN)_4]BF_4$ (94 mg, 0.30 mmol) was used in place of $Cu(BF_4)_2{\cdot}6H_2O$. Yield: 566 mg, 57%.

Method 3. A solution of MMI (137 mg, 1.20 mmol) in acetonitrile (10 mL) was transferred *via* cannula into a solution of $[Cu(CH_3CN)_4]BF_4$ (94 mg, 0.30 mmol) in acetonitrile (10 mL) under argon. The reaction was stirred for 12 h. The solvent volume was reduced by half *in vacuo*, and then diethyl ether was added to precipitate the product. The resulting white precipitate was filtered, washed with diethyl ether (10 mL), and dried *in vacuo* to give **1**. Yield: 663 mg, 67%. This reaction was also performed in air, affording **1** with a similar yield.

*2.3. Synthesis of $[Cu(\kappa^{N,N}\text{-}MMI^{MS})_2(H_2O)_2][NO_3]_2$ (**2**)*

Modifications to the published procedures of Ainscough and coworkers [30] and Lobana and coworkers [29] were made to synthesize $[Cu(\kappa^{N,N}\text{-}MMI^{MS})_2(H_2O)_2](NO_3)_2$. A solution of MMI (137 mg, 1.20 mmol) in acetonitrile (6 mL) was slowly added to a solution of $Cu(NO_3)_2{\cdot}3H_2O$ (73 mg, 0.30 mmol) in acetonitrile (5 mL), and the reaction mixture slowly turned light green. After stirring in air for 3 d, the solution became bright blue. The reaction mixture was allowed to slowly evaporate over a week to form blue crystals of **2**. Lighter blue crystals were also isolated and identified as $CuSO_4{\cdot}5H_2O$. Yield of **2**: 110 mg, 18%. The crystals were separated by hand, and confirmation of **2** was determined X-ray diffraction. The IR spectrum of **2** matched published data [29].

*2.4. Synthesis of $[Cu(\kappa^{N,N}\text{-}MMI^{MS})_2(H_2O)_2][CH_3SO_4]_2$ (**3**)*

Synthesis of *$[Cu(\kappa^{N,N}\text{-}MMI^{MS})_2(H_2O)_2][CH_3SO_4]_2$ (**3**)* was achieved through *in situ* generation of the methylsulfate ion by sulfur extrusion. Baldwin and coworkers also reported this structure in higher yields when $CuSO_4{\cdot}5H_2O$ was used as the starting material [32], although they did not report IR data for this complex. A solution of MMI (228 mg, 2.00 mmol) in acetonitrile

(10 mL) was added to a solution of $Cu(NO_3)_2 \cdot 3H_2O$ (120 mg, 0.50 mmol) in acetonitrile (10 mL). The colorless reaction mixture became blue after 1 h stirring, and a white precipitate formed. The precipitate was filtered and dried *in vacuo*, forming a highly hygroscopic solid. Upon exposure to air, water from the air was absorbed into the product. Methanol (5 mL) was added to dissolve the product, and deep blue crystals of **3** formed upon solvent evaporation in air. Darker blue crystals of **3** were manually separated from lighter blue crystals, and the imprecise elemental analysis we report is likely due to incomplete separation. Synthesis of **3** was not reproducible, despite multiple attempts, and slight modifications resulted in isolation of structurally similar complexes $[Cu(\kappa^{N,N}\text{-}MMI^{MS})_2(H_2O)][CH_3SO_4][HSO_4][H_2O]$ (**5**) and $[Cu(\kappa^{N,N}\text{-}MMI^{MS})_2(H_2O)](CH_3SO_4)_2$ (**6**). Yield of **3**: 369 mg, 52%. IR (Nujol mull, cm^{-1}): 3435 b, 3139 w, 2728 w, 1634 s, 1588 sh, 1532 w, 1487 sh, 1254 s, 1218 s, 1062 w, 1032 w, 1007 w, 960 w, 760 b, 710 sh, 655 w, 619 s, 576 w, 561 sh. Anal. Calc. for $C_{18}H_{38}CuN_8O_{10}S_4$: C, 30.10; H, 5.33; N, 15.60. Found: C, 29.32; H, 5.81; N, 15.53.

2.5. Synthesis of $[Cu(\kappa^{N,N}\text{-}MMI^{MS})_2(H_2O)_2](HSO_4)_2$ ***(4)***

While performing the EPR experiments which involved freezing the reaction solution with liquid nitrogen, small crystals were obtained in the EPR tubes. The experiment was then scaled up to obtain X-ray-diffraction-quality crystals. $Cu(NO_3)_3 \cdot 3H_2O$ (241.6 mg, 1.0 mmol) and methimazole (456 mg, 4.0 mmol) were combined in acetonitrile (30 mL), and the solution was frozen with liquid nitrogen for 5 min. Crystals of **4** grew from slow evaporation from acetonitrile. Yield: 132 mg, 21%. ESI-HRMS (*m*/*z*): $[Cu(C_3H_4N_2S)_2(H_2O)(OH)]^+$ Anal. Calc. 486.0682. Found: 486.0598. $[Cu(C_3H_4N_2S)_2]^+$ Anal. Calc. 451.0548. Found: 451.0546. IR (neat pellet, cm^{-1}): 3486 b, 3435 b, 3269 w, 3145 s, 3129, s, 2923 w, 1630 s, 1530 s, 1476s, 1413 w, 1284s, 1148 s, 847 s, 506 w.

*2.6. Synthesis of [Cu($\kappa^{N,N}$-MMI^{MS})$_2$(H_2O)][CH_3SO_4][HSO_4][H_2O] (**5**)*

A solution of MMI (137 mg, 1.20 mmol) in acetonitrile (10 mL) was slowly added to a solution of $Cu(NO_3)_2 \cdot 3H_2O$ (73 mg, 0.30 mmol) in acetonitrile (10 mL), and the reaction mixture initially turned a light green. Upon stirring for 7 d, the solution turned blue, and the solvent was removed *in vacuo* to yield a dark-blue oil. Methanol (5 mL) was added to dissolve the oil, and blue crystals of **5** formed upon evaporation in air. Synthesis of this complex was not reproducible, despite multiple attempts, most often resulting in an impure oil that could not be purified. Yield: 334 mg, 48%. IR, (Nujol mull, cm^{-1}): 3430 b, 3152 w, 3130 w, 2725 w, 2669 w, 1634 s, 1530 s, 1517 w, 1418 w, 1348 sh, 1307 w, 1286 w, 1234 s, 1147 b, 1059 s, 957 s, 867 sh, 849 s, 755 s, 708 w, 694 w, 687 w, 617 w, 581 s, 599 s, 521 w, 508 w, 460 w, 442 w.

*2.7 Synthesis of [Cu($\kappa^{N,N}$-MMI^{MS})$_2$(H_2O)](CH_3SO_4)$_2$ (**6**)*

A solution of MMI (137 mg, 1.20 mmol) in acetonitrile (6 mL) was slowly added to a solution of $Cu(NO_3)_2 \cdot 3H_2O$ (73 mg, 0.30 mmol) in dichloromethane (2 mL). As the MMI was added, a dark precipitate formed immediately and then redissolved with stirring, and the reaction mixture then turned light green. After stirring in air for 3 d, the reaction mixture turned bright blue, and a blue precipitate formed. The solution was filtered, and the isolated blue precipitate was highly hygroscopic, so the precipitate was quickly dissolved in methanol (5 mL). Diethyl ether diffusion into the methanolic solution over the period of a week yielded crystals of **6**. Yield: 123 mg, 32%. MALDI-MS (*m*/*z*): $[Cu(C_3H_4N_2S)_2]^+$ 262.3, $[Cu(C_3H_4N_2S)]^+$ 163.9. IR (Nujol, cm^{-1}) 3430 b, 2727 w, 1577 s, 1517 w, 1481 w, 1401 sh, 1246 s, 1160 w, 1108 w, 885 sh, 850 s, 768 s, 728 w, 516 w.

*2.8. Synthesis of [Cu($\kappa^{N,N}$-MMI^{MS})($\kappa^{O,O}$-SO_4)(CH_3OH)] (**7**)*

A solution of MMI (137 mg, 1.20 mmol) in acetonitrile (6 mL) was slowly added to a solution of $Cu(NO_3)_2 \cdot 3H_2O$ (146 mg, 0.60 mmol) in acetonitrile (5 mL). As MMI was added, the reaction mixture slowly turned light green. After stirring in air for 3 d, the solution turned a light blue, and the solvent was removed *in vacuo*. Methanol (5 mL) was added to dissolve the resulting oil, and crystals of **7** were obtained by slow evaporation of the methanolic solution in air. Yield: 90 mg, 13%. Synthesis of this complex was attempted multiple times but was not reproducible, resulting in structural characterization only.

*2.9. Synthesis of [Cu($\kappa^{N,N}$-MMI^{MS})($\kappa^{O,O}$-SO_4)(DMSO)]·0.5 DMSO (**8**)*

A solution of MMI (137 mg, 1.20 mmol) in acetonitrile (6 mL) was slowly added to a solution of $Cu(NO_3)_2 \cdot 3H_2O$ (73 mg, 0.30 mmol) in acetonitrile (5 mL). As MMI was added, the reaction mixture slowly turned light green. After stirring in air for 3 d, the solution turned a light green, and the solvent was removed *in vacuo*. Dimethylsulfoxide (5 mL) was added to dissolve the resulting oil, and crystals of **8** were obtained by tetrahydrofuran diffusion into the DMSO mixture. Yield: 76 mg, 16%. Synthesis of this complex was attempted multiple times but was not reproducible, resulting in structural characterization only.

*2.10. Synthesis of [Cu(μ_2,$\kappa^{O,O,O}$-SO_4)($\kappa^{N,N}$-MMI^{MS})]$_n$ · CH_3CN (**9**)*

$Cu(NO_3)_3 \cdot 3H_2O$ (241.6 mg, 1.0 mmol) and methimazole (456 mg, 4.0 mmol) were combined in acetonitrile (30 mL). Aliquots (~300 μL) were placed in 3 mm Quartz tubes, capped and EPR spectra were taken at 150 K, resulting in the freezing of the solution for 1 h. After 2 days

turquoise crystals were harvested from the EPR tube. Yield: 178 mg, 45%. ESI-HRMS (*m/z*): $[Cu(C_3H_4N_2S)]^+$ Calc.: 256.9922; found: 256.9943, $[Cu(C_3H_4N_2S)(SO_4)H]^+$ Calc.: 353.9518; found: 353.9604, $[Cu_2(C_3H_4N_2S)_2(SO_4)H]^+$ Calc. 619.9440; found: 610.9503, $[Cu_2(C_3H_4N_2S)_2(SO_4)_2H]^+$ Calc:. 706.8958; found: 706.9048. IR (neat pellet, cm^{-1}): 3298 b, 3104 w, 2934 w, 1640 w, 1529 s, 1489 s, 1418 sh, 1284 s, 1158 w, 1121 s, 883 sh, 799 s, 658 w.

2.11. X-ray crystallography

Single crystal X-ray diffraction measurements were performed at 100 K using Mo Kα (λ = 0.71073 Å radiation on a Bruker D8 Venture diffractometer with an Incoatec microfocus source and a Photon 100 CMOS detector. The Apex3 software suite was used for data collection, processing, and scaling corrections [37]. A summary of crystallographic data for **1, 10,** and **11** is available in Table S1, data for **2-5** are in Table S2, and data for **6-9** are in Table S3. Space group assignments were made based on systematic absences. Structures were solved by intrinsic phasing (SHELXT), and refined to convergence by full-matrix least squares using the SHELXTL software suite [38]. All non-hydrogen atoms were refined anisotropically. Hydrogen atoms attached to carbon atoms were placed geometrically and treated using appropriate riding models. Positions of hydrogen atoms attached to nitrogen and oxygen atoms were first verified using the difference electron density maps, and then placed in geometrically optimized positions using riding models. The final positions of these hydrogen atoms did not differ significantly from where their position was first indicated on the difference electron density map.

Several structures in the present study required somewhat special treatment during the refinement process. In the case of **10**, the nitrate counterion and methanol solvent molecule were found to be disordered in several different orientations. Thus, their electron density was best modeled using the SQUEEZE algorithm in the PLATON software package [39]. For **5**, the methyl

sulfate counterion was modeled in two disordered orientations, each with 50% occupancy. In **8**, the coordinated DMSO molecule was found to be disordered, with the sulfur and carbon atoms modeled over split positions and the occupancy values for the two disordered orientations refined as free variables. The only noncentrosymmetric structure in the present study is that of **9**, which was found to crystallize in the polar space group *Cm*. In this case the Flack parameter of 0.054(10) supports the correct absolute structure.

2.12. EPR spectroscopy

To prepare EPR samples, $Cu(NO_3)_3 \cdot 3H_2O$ (241.6 mg, 1.0 mmol) and methimazole (456 mg, 4.0 mmol) were combined in acetonitrile (30 mL). Aliquots (~300 μL) were taken immediately after mixing and after 1, 3 and 20h. 5,5-Dimethyl-1-pyrroline-*N*-oxide (DMPO, 66 mM) was added to all the RT samples as a spin trap. EPR spectra were measured on a Bruker EMX spectrometer at room temperature and 150 K in 3 mm quartz tubes. For the experiments at room temperature, spectra centered at 3511.75 G were acquired with a sweep width of 200 or 1500 G. The modulation amplitude was 1.00 G with time and conversion constants of 163.84 s, and microwave power and frequency were 2.002 mW and 9.752 GHz, respectively. Experiments as 150 K were conducted on samples flash-frozen in liquid nitrogen with spectra centered at 3000 G with a sweep with of 2000 G. The modulation amplitude was 1 G with time and conversion constants of 163.84 s, and microwave power and frequency were 2.002 mW and 9.435 GHz, respectively. EasySpin (Version 5.2.25) in MatLab (Version R2019a) was used to simulate the 150K EPR spectra [40], and WinSim [41] was used to simulate EPR spectra obtained at room temperature.

3. Results and Discussion

3.1. Synthesis

Two variables were analyzed when exploring reactions between copper and methimazole: the oxidation state of the copper and the presence of oxygen. To determine the effect of the oxidation state of copper in the reaction, separate reactions of $[Cu(NCCH_3)_4][BF_4]$ or $Cu(BF_4)_2$ with methimazole in acetonitrile were performed (Scheme 2). In both reactions, the previously reported complex [23], $[Cu^{I}_2(\mu,\kappa^{S}\text{-MMI})_2(\kappa^{S}\text{-MMI})_4][BF_4]_2$ (**1**) was produced as the primary product (Scheme 2). Sulfur extrusion has been reported under similar conditions to form the $[Cu^{II}(\kappa^{N,N}\text{-MMI}^{MS})_2(H_2O)_2][BF_4]_2$ product [29], but under the conditions examined in this work, the dinuclear Cu^+ complex, **1**, was found to be very stable, even in air. With $Cu(BF_4)_2$ as the copper source, the blue reaction solution becomes colorless, indicating reduction of Cu^{2+} to Cu^+, with concomitant formation of MMI^{DS} (Scheme 2B), and **1** was isolated as a white solid in 36% yield. Formation of MMI^{DS} in addition to **1** was verified by MALDI-MS of the reaction solution (*m*/*z* 227 for $[MMI^{DS}H]^+$), but no Cu^+-coordinated MMI^{DS} product was isolated. Raper [22] previously synthesized complex **1** from $Cu(BF_4)_2$ using similar methods, but MMI^{DS} formation during the reaction was not examined. Although O_2 was readily available during the synthesis in air, there was no indication of sulfur elimination with acetonitrile as the solvent and tetrafluoroborate as the counterion, either in analysis of the reaction mixture by MALDI-MS or in the isolated products.

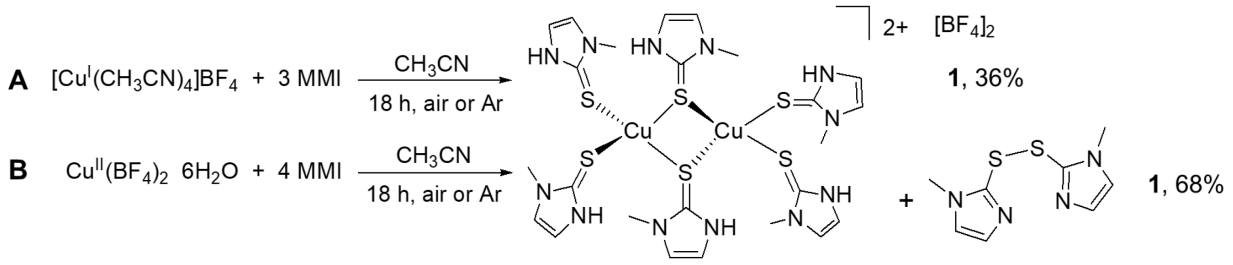

Scheme 2. Reaction conditions used to evaluate the effects of copper oxidation state and counterions on product formation. Scheme 2A results in formation of only dinuclear **1** in 68% yield, and Scheme 2B results in formation of **1** as well as the oxidized methimazole dimer.

Sulfur extrusion to form copper-coordinated MMI^{MS} ligands is consistently observed for reactions performed in air with $Cu(NO_3)_2$ as the copper source [27,29,30,32,33]. For this study, a variety of conditions were pursued in an attempt to reproduce previous results [29]. Upon addition of methimazole in acetonitrile to $Cu(NO_3)_2{\cdot}3H_2O$ in methanol in a 4:1 ligand to metal ratio, the blue Cu^{2+} solution turns light yellow, indicating the reduction of the copper ion to Cu^{+}. After stirring for 12 h, the solution turns back to light blue, suggesting oxidation of Cu^{+} back to Cu^{2+} by oxygen. After stirring for 3 d, products were isolated under a variety of conditions using several different solvents (Scheme 3). We obtained complex $[Cu^{II}(\kappa^{N,N}\text{-}MMI^{MS})_2(H_2O)_2][NO_3]_2$ (**2**) reported previously by Ainscough [30] and Lobana [42] by ether diffusion into the reaction mixture. The complex $[Cu^{II}(\kappa^{N,N}\text{-}MMI^{MS})_2(H_2O)_2][CH_3SO_4]_2$ (**3**) [32], as well as the novel $[Cu^{II}(\kappa^{N,N}\text{-}MMI^{MS})_2(H_2O)][CH_3SO_4][HSO_4]{\cdot}H_2O$ (**5**) are obtained by solvent evaporation. $[Cu^{II}(\kappa^{N,N}\text{-}MMI^{MS})_2(H_2O)][CH_3SO_4]_2$ (**6**) is obtained by slow evaporation after a reaction time of only 18 h. The sulfate-bound $[Cu^{II}(\kappa^{N,N}\text{-}MMI^{MS})(\kappa^{O,O}\text{-}SO_4)(CH_3OH)]$ (**7**) complex is obtained when the ligand-to-metal ratio was reduced to 2:1, and $[Cu(\kappa^{N,N}\text{-}MMI^{MS})(\kappa^{O,O}\text{-}SO_4)(DMSO)]{\cdot}0.5$ DMSO (**8**) is obtained under similar conditions when the solvent was varied. In the process of analyzing the reaction progress by EPR spectroscopy, yet another product was obtained, $[Cu(\mu_2,\kappa^{O,O,O}\text{-}SO_4)(\kappa^{N,N}\text{-}MMI^{MS})]_n$ $[CH_3CN]$ (**9**). Reaction conditions were identical to those shown in Scheme 3, but the solution was initially frozen at 150 K before solvent evaporation and product isolation. MALDI-MS results of the reaction solutions confirm the presence of Cu-MMI and Cu-MMI^{DS} fragments, but no evidence of MMI^{MS} formation is observed.

As is evident from the relatively similar reaction conditions and wide variety of products obtained, the outcome of this reaction is very dependent upon the synthetic environment. Many of these products were obtained in poor yield (**4**, **6-9**), and characterization for several (**3**, **7**, **8**) is

$Cu(NO_3)_2 \cdot 3H_2O + n$ MMI $\xrightarrow{CH_3CN/CH_3OH}$

(**2**) n=**4**, 3 d, ether diffusion	$[Cu^{II}(\kappa^{N,N}\text{-MMI}^{MS})_2(H_2O)_2][NO_3]_2$	**2**, 32%
(**3**) n=**4**, 3 d, evaporation	$[Cu^{II}(\kappa^{N,N}\text{-MMI}^{MS})_2(H_2O)_2][CH_3SO_4]_2$	**3**, 48%
(**4**) n=**4**, frozen 15 min, evaporation	$[Cu^{II}(\kappa^{N,N}\text{-MMI}^{MS})_2(H_2O)_2][HSO_4]_2$	**4**, 21%
(**5**) n=**4**, 3 d, evaporation	$[Cu^{II}(\kappa^{N,N}\text{-MMI}^{MS})_2(H_2O)][CH_3SO_4][HSO_4]$	**5**, 52%
(**6**) n=**4**, 18 h, evaporation	$[Cu^{II}(\kappa^{N,N}\text{-MMI}^{MS})_2(H_2O)][CH_3SO_4]_2$	**6**, 29%
(**7**) n=**2**, 3 d, ether diffusion	$[Cu^{II}(\kappa^{N,N}\text{-MMI}^{MS})(\kappa^{O,O}\text{-}SO_4)(CH_3OH)]$	**7**, 13%
(**8**) n=**2**, 3 d, DMSO/THF diffusion	$[Cu^{II}(\kappa^{N,N}\text{-MMI}^{MS})(\kappa^{O,O}\text{-}SO_4)(DMSO)]$	**8**, 18%
(**9**) n=**4**, frozen 1 h, evaporation	$\{[Cu^{II}(\kappa^{N,N}\text{-MMI}^{MS})(\mu^2,\kappa^{O,O,O}\text{-}SO_4)\}_n$	**9**, 43%

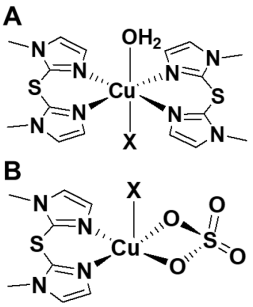

Scheme 3. Treating methimazole (MMI) with $Cu(NO_3)_2$ under aerobic conditions results in a variety of sulfur-extruded, MMI^{MS}-containing products. Complexes **2**, **3**, and **4** have two axial ligands (X = OH_2), resulting six-coordinate complexes with the A structure), whereas complexes **5** and **6** have one axial ligand (no X), resulting 5-coordinate complexes. Complexes **7** and **8** are 5-coordinate with the B structure (X = CH_3OH and DMSO, respectively), and complex **9** has the B structure with X = a third oxygen of SO_4 from another $Cu(\kappa^{N,N}\text{-MMI})_2(\kappa^{O,O}\text{-}SO_4)$ center to form a coordination polymer. X-ray diffraction structures of **4**, **5**, **7**, **8**, and **9** are provided in Figs. 2 and 3.

lacking due to difficulties in reproducing the products that were confirmed by X-ray structural analysis. Obtaining elemental analyses also was challenging for some products (**3**), likely due to co-crystallization of these very similar products. What is consistent for these similar complexes is that the MMI^{MS} ligand as well as HSO_4^- and $CH_3SO_4^-$ counterions are generated *in situ*, and that these reaction products depend on oxygen, water, and/or methanol availability. Although water was never directly used as a solvent, water molecules were present in the copper hydrate starting materials and, in some cases, may have been absorbed from the air during solvent evaporation. The critical dependence of solvent is evident in the observed Cu-solvato coordination in these complexes.

Although sulfate or methylsulfate ions were not present in the starting materials of the reactions that yielded complexes **2-9**, sulfate and methylsulfate counterions are observed in the isolated products. This suggests that these counterions form from oxidation of the extruded sulfur during the course of the reaction. In cases where only two equivalents of MMI were present, one of the two Cu^{2+}-coordinated MMI^{MS} ligands (observed in complexes **2-8**) is replaced with Cu^{2+}-

coordinated sulfate in complexes **7-9**. In the reported synthesis of **3** [32], copper(II) sulfate was used as a reactant, so the source of the methylsulfate could not be positively identified.

To examine the oxygen dependence of MMI^{MS} formation, $Cu(NO_3)_2$ and methimazole were combined under air-free conditions (Scheme 4). Upon $Cu(NO_3)_2$ addition, the blue reaction mixture immediately became colorless, indicating Cu^{2+} reduction to Cu^{+} by methimazole. MMI^{DS} formation was confirmed by MALDI-MS analysis of the reaction mixture. The reported mononuclear complex $[Cu(MMI)_3][NO_3]$ [19] was obtained and its synthesis was confirmed by X-ray structural analysis and IR spectroscopy. A unique polymer, $\{[Cu(\mu,\kappa^S\text{-MMI})(\kappa^S\text{-MMI})](NO_3)\}_n$ (**10**, 10% yield) was obtained and confirmed by single crystal X-ray diffraction, but this synthesis could not be reproduced. Full synthetic details and characterization of this product and a similar polymer, $\{[Cu_2(\mu,\kappa^S\text{-HMI})_3](NO_3)_2\}_n$ (**11**), resulting from the reaction of $Cu(NO_3)_2$ with 2-mercaptoimidazole (HMI; Scheme 4B) are provided in the Supporting Information. No evidence for sulfur extrusion is observed under oxygen-free conditions, since both the mononuclear $[Cu(MMI)_3][NO_3]$ and polymeric **10** involve direct coordination of the methimazole ligand to Cu^{+}.

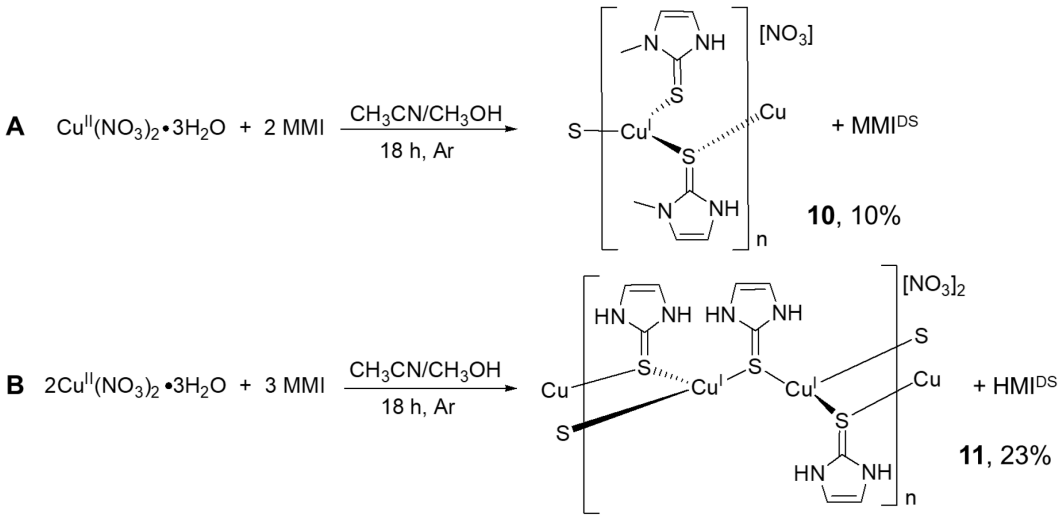

Scheme 4. When the reaction between $Cu(NO_3)_2$ and imidazole thiones, MMI and HMI, were performed under air-free conditions, the sulfur-bridging coordination polymers, $\{[Cu(\mu,\kappa^S\text{-MMI})(\kappa^S\text{-MMI})](NO_3)\}_n$ (**10**) and $\{[Cu_2(\mu,\kappa^S\text{-HMI})_3](NO_3)_2\}_n$ (**11**), respectively, were obtained.

From the reactions shown in Schemes 2, 3, and 4 it is evident that oxygen availability, copper ionization state, counterion availability, and solvent effects all influence the products formed with these relatively simple reactants. Cu^{+} forms complexes with the thione sulfur of MMI, as seen in complexes **1** and **10**, but control of oxygen is crucial. Sulfur extrusion is only observed under aerobic conditions, as exemplified by complexes **2-9**. Although disulfide oxidation to sulfinates or sulfonates is fairly common [34,43-45], sulfur elimination has only been reported for MMI reactions. The identity of the metal also plays a critical role. Complexes with imidazole disulfide ligands have been reported with a variety of metals: Co(*t*-butyl-MMI^{DS})$_2Cl_2$ [46], Zn(*t*-butyl-MMI^{DS})$_2Cl_2$ [47], Fe(*t*-butyl-MMI^{DS})$_2Cl_2$ [47], Ni(*t*-butyl-MMI^{DS})$_2Cl_2$ [47], and Zn(MMI^{DS})Cl_2 [48], but no copper complexes with the disulfide ligand, MMI^{DS}, have been reported. All these complexes were synthesized under aerobic conditions with no evidence of sulfur oxidation or elimination. Aside from the halide-bridging, dinuclear, [Cu^{II}_2($\kappa^{N,N}$-MMI^{MS})$_2$(μ-Cl)$_2$)Cl_2 [29,33] no other metal complexes with the MMI^{MS} ligand are reported, although sulfur extrusion to form the monosulfide diimmidazole, 2,2'-thio-di-2-imidazoline, was observed when hydrotris(thioimdazolyl) borate was treated with iodine [49] and in the reaction of CuCl with HMI [42].

Redox-active copper and oxygen availability consistently lead to sulfur elimination and the *in situ* generation and coordination of MMI^{MS}. Subsequent Cu^{2+} coordination of the monosulfide (MMI^{MS}) is favored in a bidentate fashion in the equatorial position, with a variety of solvato ligands coordinating in the axial positions. Disulfide oxidation to sulfinate is common [34,43,44], but this generally results in the breaking of the disulfide bond rather than complete oxidation and elimination of a sulfur atom. The presence of methylsulfate ions in **3**, **5**, and **6** indicates that nucleophilic attack of methanol on a sulfur atom may occur prior to sulfur elimination.

3.2. Structural analysis of Cu-methimazole complexes

Single-crystal X-ray diffraction data were collected for the eight different complexes examined in this work that incorporate the sulfur-extruded MMI^{MS} ligand: $[Cu^{II}(\kappa^{N,N}\text{-}MMI^{MS})_2(H_2O)_2][NO_3]_2$ (**2**), $([Cu^{II}(\kappa^{N,N}\text{-}MMI^{MS})_2(H_2O)_2][CH_3SO_4]_2$ (**3**), $([Cu^{II}(\kappa^{N,N}\text{-}MMI^{MS})_2(H_2O)_2][H_2SO_4]_2$ (**4**), $[Cu^{II}(\kappa^{N,N}\text{-}MMI^{MS})_2(H_2O)][CH_3SO_4][HSO_4]\cdot H_2O$ (**5**), $([Cu^{II}(\kappa^{N,N}\text{-}MMI^{MS})_2(H_2O)][CH_3SO_4]_2$ (**6**), $Cu^{II}(\kappa^{N,N}\text{-}MMI^{MS})(\kappa^{O,O}\text{-}SO_4)(CH_3OH)$ (**7**), $Cu(\kappa^{N,N}\text{-}MMI^{MS})(\kappa^{O,O}\text{-}SO_4)(DMSO)\cdot 0.5$ DMSO (**8**), and $\{Cu^{II}(\kappa^{N,N}\text{-}MMI^{MS})(\kappa^{O,O}\text{-}SO_4)\}_n(CH_3OH)$ (**9**) Most of these Cu^{2+} complexes can be grouped into three categories based on the copper coordination in the cationic complexes: 1) octahedral geometry with two MMI^{MS} ligands in the equatorial positions bound in a bidentate fashion through the nitrogen atoms and having two water molecules coordinated in the axial positions (**2**-**4**), 2) distorted square pyramidal geometry with two MMI^{MS} ligands in the equatorial positions and one water molecule in the axial position (**5** and **6**), and 3) distorted square pyramidal geometry with one MMI^{MS} ligand in the equatorial position, one bidentate sulfate dianion in the equatorial position, and a coordinated solvent molecule (methanol or DMSO) in the axial position (**7** and **8**). Since the structure of **2** and **3** are published [29], but the data reported here represents an improved refinement of **3** (Table S2). Our data will be used for structural analysis for a consistent comparison of structures. The cation of complex **4** is structurally similar to **2** and **3** [32] but with a different counterion (HSO_4^-) and will be used as a representative cation with octahedral coordination to compare to **5** and **6** as well as for general discussion of the fate of the extruded sulfur. The cation structures with octahedral coordination (**2**-**4**) and those with square pyramidal geometry (**5** and **6**) are shown in Figure 2. Bond lengths and angles are given in Table 1 for complexes **2**-**6**.

Complexes **7** and **8** exhibit distorted square pyramidal geometry and coordinate only one

molecule of MMI^{MS} in an equatorial position (Figure 2 and Table 2). Equatorial coordination is completed by bidentate coordination of a sulfate group, although the equatorial plane is distorted due to the ring strain inherent in the 4-membered chelate ring formed by the sulfate with copper. A solvent molecule coordinates in the axial position for both **7** (CH_3OH) and **8** (DMSO), varying depending on the crystallization solvent. All of these products are solvent-dependent, since H_2O,

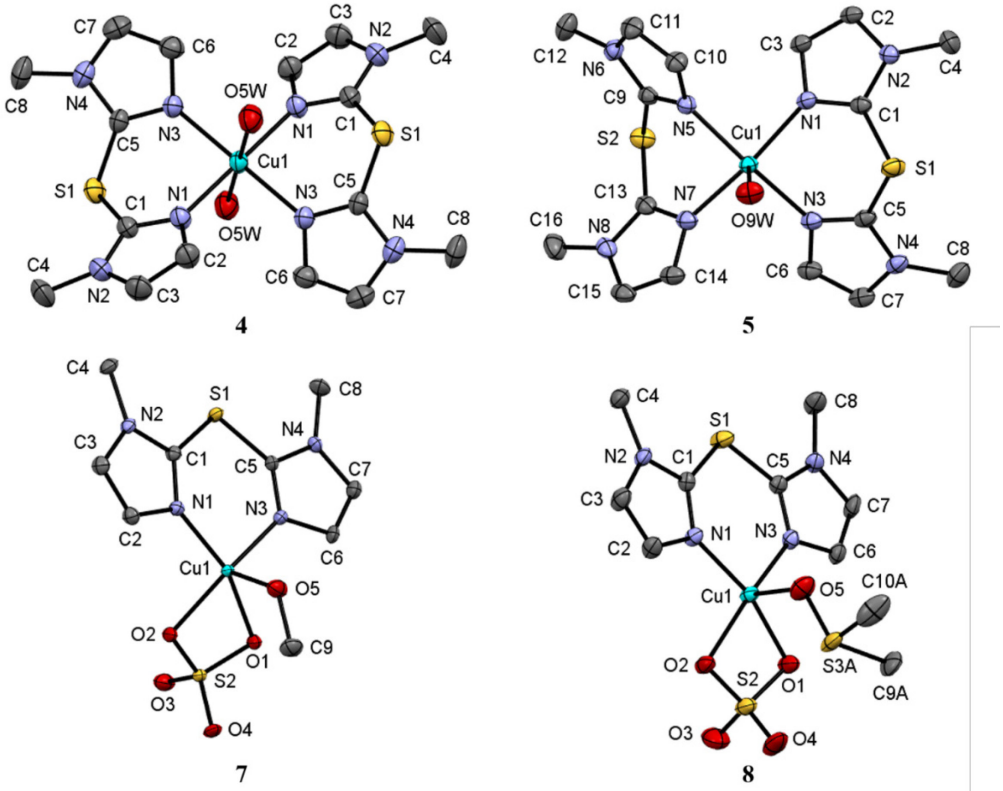

Figure 2. Representative structures of the various coordination patterns in the Cu^{2+} complexes of the present study, shown as 70% probability density ellipsoids. The octahedral coordination exhibited by **4** is also demonstrated by **2** and **3**, and the square pyramidal coordination exhibited by **5** is also exhibited by **6**. Hydrogen atoms, non-coordinated solvent molecules, and counterions are omitted for clarity.

Table 1. Selected bond lengths (Å) and angles (˚) for $[Cu(\kappa^{N,N}\text{-}MMI^{MS})_2(H_2O)_x]^{2+}$ complexes **2**, **3**, **4**, **5**, and **6** with x = 2 for **2**-**4** and x = 1 for **5** and **6**. In **2**-**4**, only half of the complex is unique, while in **5** and **6** the entire complex is unique.

	2	**3**	**4**	**5**	**6**
Cu-N	2.0171(12) (x2)	2.000(2) (x2)	2.0072(13) (x2)	1.9969(17)	1.9943(18)
	2.0172(12) (x2)	2.002(2) (x2)	2.0120(13) (x2)	1.9972(17)	1.9978(17)
				1.9998(17)	2.0003(18)
				2.0115(18)	2.0034(18)
Cu-O(water)	2.4514(12) (x2)	2.4186(19) (x2)	2.4639(14) (x2)	2.1926(16)	2.1864(16)
C-S	1.7474(15) (x2)	1.760(3) (x2)	1.7476(16) (x2)	1.746(2)	1.748(2)
	1.7520(15) (x2)	1.768(3) (x2)	1.7491(16) (x2)	1.751(2)	1.751(2)
				1.758(2)	1.755(2)

				1.759(2)	1.756(2)
N-Cu-N (trans)	180 (x2)	180 (x2)	180 (x2)	163.47(7)	165.80(7)
				169.86(7)	169.20(7)
N-Cu-N (cis)	88.42(5) (x2)	89.06(9) (x2)	88.09(5) (x2)	87.16(7)	87.62(7)
	91.58(5) (x2)	90.94(9) (x2)	91.91(5) (x2)	88.17(7)	88.41(7)
				89.85(7)	89.33(7)
				91.97(7)	92.01(7)
N-Cu-O(water)	86.38(4) (x2)	87.12 (8) (x2)	88.24(5) (x2)	90.86(7)	93.67(7)
	88.61(5) (x2)	89.21(8) (x2)	89.50(5) (x2)	96.31(7)	96.77(7)
	91.39(5) (x2)	90.79(8) (x2)	90.50(5) (x2)	99.27(7)	97.10(7)
	93.62(4) (x2)	92.88(8) (x2)	91.76(5) (x2)	100.09(7)	97.37(7)

Table 2. Selected bond distances (Å) and angles (˚) for $[Cu(\kappa^{N,N}\text{-}MMI^{MS})(\kappa^{O,O}\text{-}SO_4)(L)]^{2+}$ complexes. For **7**, L = CH_3OH and for **8**, L = DMSO).

	7	**8**
Cu-N1	1.9547(16)	1.957(3)
	1.9587(16)	1.959(3)
Cu-O(sulfate)	2.0078(13)	1.992(2)
	2.0083(13)	1.997(3)
Cu-O(solvent)	2.2186(15)	2.259(3)
C-S	1.7473(19)	1.744(4)
	1.7493(18)	1.746(4)
N-Cu-N	93.40(6)	93.95(13)
N-Cu-O(sulfate)	159.78(7)	160.00(12)
	160.84(6)	165.65(12)
	95.31(6)	94.65(12)
	95.41(6)	96.85(12)
N-Cu-O(solvent)	100.35(6)	91.97(12)
	100.82(6)	101.05(12)
O(sulfate)-Cu-O(sulfate)	71.29(6)	71.73(11)
O(sulfate)-Cu-O(solvent)	94.35(6)	95.36(12)
	95.82(6)	97.62(11)

CH_3OH, and DMSO stabilize the axial positions of the five-coordinate or six-coordinate complexes. The coordinated aquo ligands likely are from the waters of hydration of the $Cu(NO_3)_2{\cdot}3H_2O$ starting material, since dry solvents were used for all the synthetic and purification steps.

Although unique in the polymeric structure, $[Cu(\mu_2,\kappa^{O,O,O}\text{-}SO_4)(\kappa^{N,N}\text{-}MMI^{MS})]_n$ $[CH_3CN]$ (**9**), demonstrates similar characteristics to structures **7** and **8**. As with these complexes, the central Cu^{2+} ion exhibits distorted square pyramidal coordination by one bidentate MMI^{MS} ligand in the equatorial position and one bidentate sulfate ion also in the equatorial position (Figure 3). The axial position is occupied by the oxygen atom of the next sulfate group in the polymeric chain, as

the sulfate ions form the backbone of the polymeric structure. In this way, three oxygen atoms from the sulfate group coordinate a total of two copper atoms to propagate the chain. The one non-copper-coordinating oxygen atom still contributes to the stabilization of the crystal structure by acting as a hydrogen-bonding acceptor from methimazole ligands in neighboring chains as well as the non-coordinated acetonitrile solvent molecule. Bond lengths and bond angles for **9**

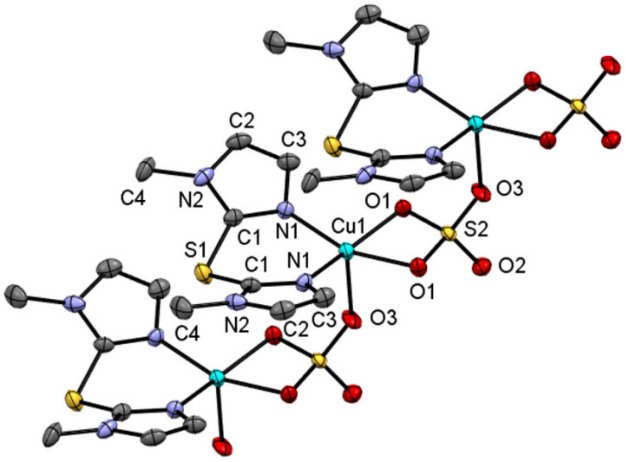

Figure 3. Crystal structure of **9** shown as 50% probability density ellipsoids. Hydrogen atoms and non-coordinated solvent molecules are omitted for clarity.

are given in Table S6.

Single crystal X-ray diffraction data were also collected for the Cu^{+} complexes, $[Cu^{I}_2(\mu,\kappa^{S}\text{-MMI})_2(\kappa^{S}\text{-MMI})_4][BF_4]_2$ (**1**), $\{[Cu(\mu,\kappa^{S}\text{-MMI})(\kappa^{S}\text{-MMI})](NO_3)\}_n$ (**10**), and $\{[Cu_2(\mu,\kappa^{S}\text{-HMI})_3](NO_3)_2\}_n$ (**11**), and structural parameters are given in Table S1. X-ray data for **1** is consistent with previous reports [23], although our unit cell dimensions are slightly smaller (Table S1) and the structure is free from $(BF_4)^{-}$ disorder, likely due to structural determination at a lower temperature (100 K). Since the Cu^{I}-methimazole complex **1** is reported and coordination polymers **10** and **11** were not reproducible products, discussion of these structures is provided in the Supporting Information.

For all of the structures, little change is observed in the C-S bond length (1.75 Å), whether the methimazole S is terminal (**1**)**,** bridging (**10**), or in the monosulfide ligands (**2**-**9**). This bond length is significantly longer than the C=S bond in uncoordinated methimazole (1.686 Å) [50] or dimethylimidazole thione (1.698 Å) [51], and is shorter than the C-S single bonds of thiols (1.86 Å). This suggests that the C-S bond is an extension of the electron delocalization exhibited in the heterocycle. Furthermore, the bond length of the non-methylated nitrogen of the imidazole ring and sulfur-bound carbon shortens upon complexation as compared to the protonated unbound ligand. This shortening and lack of electron density supports the supposition that electron density is shifted to the ring as the methimazole coordinates copper in all complexes. Under all conditions, the thione exhibits a remarkable capacity to bridge copper ions. As demonstrated by the Cu^{+} coordination polymer structures, the imidazole moiety also increases stability to the three-dimensional structure through π-stacking (see Supporting Information).

3.3. Elucidating the sulfur extrusion mechanism

Sulfur extrusion is observed for all reactions performed in air with the $Cu(NO_3)_2$ starting material (Scheme 3). MMI^{DS} initially forms as the Cu^{2+} is reduced by MMI (Scheme 1); however, in the reaction and/or crystallization process, a sulfur atom is eliminated from the disulfide, and the resulting MMI^{MS} coordinates Cu^{2+}. Previous groups have attributed oxidation of the disulfide bond to either water [44] or dioxygen exposure [29]. Subsequent sulfur elimination is only observed in the presence of strong oxidizers [52,53] or in the presence of electron-rich transition metals [29-33,42,54]. The most detailed mechanism for sulfur extrusion from MMI^{DS} to form MMI^{MS} was proposed by Lobana and coworkers [29], but this mechanism fails to 1) incorporate the critical role of copper coordination, 2) does not address stoichiometry in the oxidation of the

sulfur, and 3) does not address the role of the solvent in the formation of the methyl sulfate counterion.

A complete mechanism for this sulfur extrusion reaction is provided in Scheme 5. As in the mechanism proposed by Lobana, oxidation of MMI to MMI^{DS} is facilitated by Cu^{2+} reduction to Cu^{+} followed by Cu^{+} coordination to MMI^{DS}. Although no copper-MMI^{DS} structure is reported, a structure in which a trigonal Cu^{+} coordinates to the N atoms of a *N*-*t*-butyl-substituted imidazole disulfide, very similar to MMI^{DS}, is reported by Figueroa and coworkers [47]. This imidazole disulfide complex was synthesized under air-free conditions and features a trigonal planar Cu^{+} complex of the bidentate imidazole disulfide with a chloride or iodide in the third position. Bidentate *N*,*N*-coordination of metal ions with similar heterocyclic disulfides is observed for a wide variety of metal ions, including Zn^{2+} coordination to MMI^{DS} in a bidentate fashion [47,48], similar to the Cu+-MMI^{DS} coordination in Scheme 5.

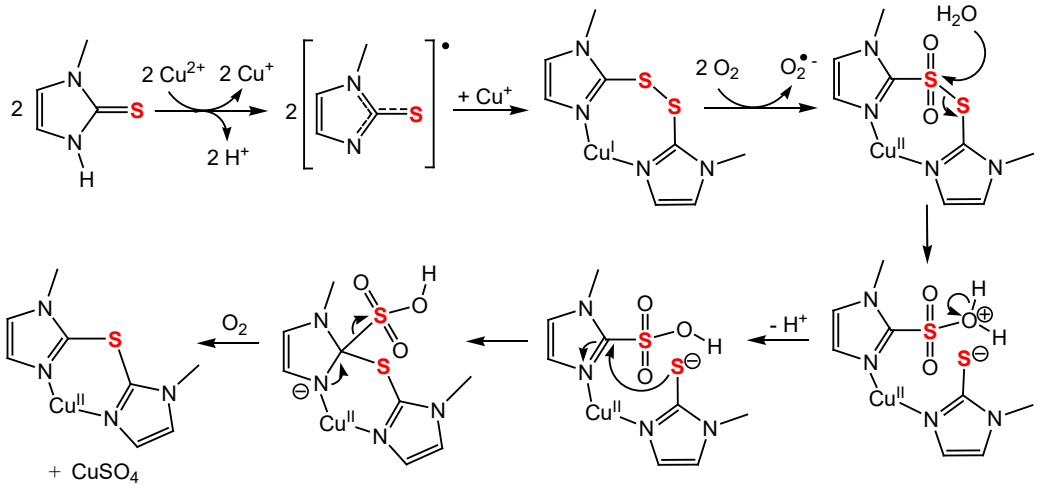

Scheme 5. New mechanism for formation of MMI^{DS} by Cu^{2+} reduction, formation of the sulfone by reaction with dioxygen, and eventual sulfur extrusion via nucleophilic aromatic substitution.

Cu^{2+} (d^9) is readily observed using EPR spectroscopy, whereas Cu^{+} (d^{10}) is EPR silent. Thus, this method is ideal for observing copper redox chemistry and for determining Cu^{2+} coordination modes, since Cu^{2+} *g* values are sensitive to coordination geometry and electronic

contributions of the ligands [55,56]. When Cu^{2+} (as $Cu(NO_3)_2$) and 4 equiv MMI were combined in acetonitrile, EPR spectra collected at 150 K show initial tetrahedral coordination of Cu^{2+} by four sulfur atoms of the MMI ligands (Figure 4; $g_\perp = 2.01$, $A_\perp = 30$ G; $g_\parallel = 2.16$, $A_\parallel = 129.9$ G) [57]. The resonances for this species can still be detected after 1 h as resonances for a second species consistent with a planar or octahedral $Cu^{II}N4$ or $Cu^{II}N6$ species appear (Figure 4) [55,57]; both species are also detected in copper EPR spectra acquired at room temperature (Figure S3). After

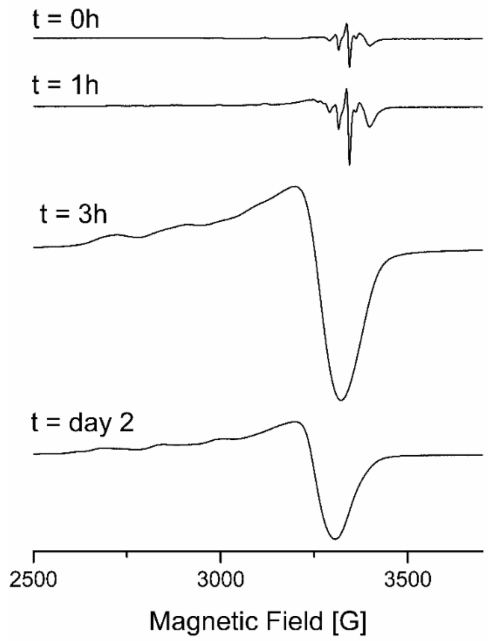

Figure 4. EPR spectra at 150 K of $Cu(NO_3)_2$ and MMI in acetonitrile taken immediately and after 1, 3, and 20 h.

3 h, resonances from the first CuS4 species are no longer present, and resonances for the $Cu^{II}N4$ or $Cu^{II}N6$ species are observed that do not change significantly after 20 h (Figure 4; $g_\perp = 2.0$, $A_\perp = 227$ G; $g_\parallel = 2.25$, $A_\parallel = 190$ G).

To determine whether non-copper-based radical species are produced, room temperature EPR spectroscopy was performed on $Cu(NO_3)_2$/MMI samples in acetonitrile in the presence of DMPO, a spin trap that reacts with radical species, including hydroxyl radical and superoxide [58]. Immediately after mixing, DMPO radical adduct signals are observed that increase in intensity

until 1 h (Figure 5) and are not observed at 3 h. These resonances are consistent with simulations of a mixture of two radical species, both DMPO-MMI adducts, one bound through the imidazole nitrogen (a_N = 16.395 G, a_H = 13.366 G, a_N = 2.865 G;) and one through the sulfur (a_N = 9.324, a_H = 10.760 G). This is the first report of radical species being formed upon the reaction of MMI with Cu^{2+}.

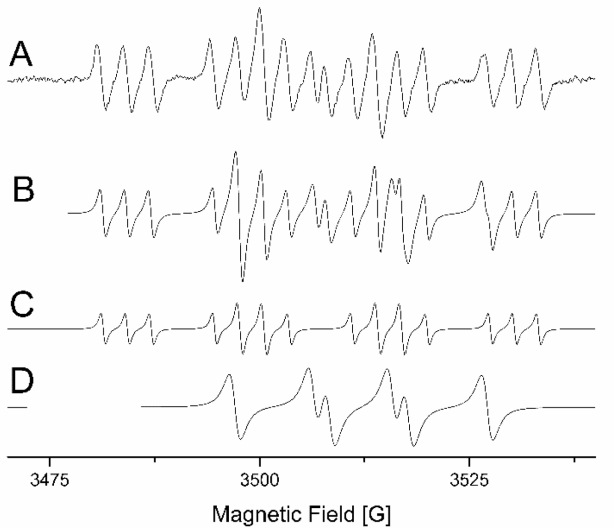

Figure 5. EPR spectrum and simulations of $Cu(NO_3)_2$/MMI at room temperature in acetonitrile: A) experimental spectrum, B) simulated spectrum with *S*- and *N*-bound MMI-DMPO adducts, C) simulated *N*-bound DMPO-MMI adduct, and D) simulated *S*-bound DMPO-MMI adduct.

These EPR results indicate that the initial step of the Cu^{2+} reaction is coordination of MMI to copper, followed by homolytic bond cleavage to form the thiyl radical and reduce Cu^{2+} to Cu^{+} with MMI deprotonation. Due to the tautomeric nature of the radical, two different DMPO adducts are observed in a 62:38 ratio for the *N*-DMPO and *S*-DMPO radical adducts based on EPR simulations. A similar DMPO-cysteine thiyl adduct has been reported by Harman *et al*. [59]. The MMI thiyl radical then reacts with another thiyl radical, forming the disulfide bond, and Cu^{+} coordinates to the nitrogens of the MMI^{DS} (Scheme 5). Similar formation of thiyl radicals has been thoroughly studied in the reaction of Cu^{2+} with cysteine that generates oxidized cysteine [60] as well as with glutathione [61,62] and penicillamine [63]. For the copper-cysteine reaction, Graf et

al. [60] reported that more thiyl radicals formed with a 1:1 ratio of cysteine to copper than at higher cysteine-to-copper ratios.

After 20 h, weak EPR resonances are detected for the DMPO-OH or DMPO-OOH adduct (Figure 4); these species cannot be distinguished due to weak signal-to-noise. Both of these species form when superoxide reacts with DMPO [58], since the DMPO-OH adduct is a known decomposition product of the short-lived DMPO-OOH adduct ($t_{1/2}$ = 65s) [64,65].

Lobana *et al*. [29] proposed that the initial step of the reaction involves Cu^{2+}-methimazole coordination, but we present the first real-time characterization of this step, identifying the $Cu^{II}S4$ complex that is initially formed, followed by a change in coordination to $Cu^{II}N4$. Although Cu^{+} cannot be directly observed in EPR spectra, formation of **1**, even with $Cu^{II}(BF_4)_2$ as the starting material, supports reduction of $Cu^{II}S4$ to $Cu^{I}S4$ as MMI^{DS} forms. Subsequent oxidation of the Cu^{+} back to Cu^{2+} and its coordination to the nitrogen atoms of the MMI^{DS} is confirmed by formation of a $Cu^{II}N4$ species by EPR spectroscopy.

In the presence of oxygen, one of the MMI^{DS} sulfur atoms is then oxidized to the sulfone, a product observed by mass spectrometry [29] with concomitant oxidation of Cu^{+} to Cu^{2+}. Nucleophilic attack by water or methanol on the sulfone sulfur then initiates rupture of the S-S bond to form an imidazole thiolate. A similar mechanism of sulfur elimination has been proposed in a recent publication by Rai and coworkers [66], in which the sulfur is completely eliminated from heterocyclic thiones through H_2O_2 oxidation. In this step, Cu^{2+} coordination is likely required to keep the nucleophilic imidazole thiolate in proximity to the now-separated, second imidazole ring. Nucleophilic attack by the imidazole thiolate then occurs, eliminating the extruded sulfur as sulfite or methylsulfite. Sulfite oxidation to sulfate catalyzed by transition metals is well known [67,68], and in this case, possible formation of superoxide may also contribute to sulfite oxidation.

Nucleophilic attack by water or methanol on the oxidized sulfur to ultimately generate sulfate or methylsulfate ions after the nucleophilic aromatic substitution and subsequent oxidation of the extruded sulfur is consistent with sulfate and methylsulfate formation observed in complexes **6-10**. Overall, the nucleophilic aromatic substitution portion of the mechanism is similar to that observed for thiolate deprotection of nitrobenzenesulfonyl [69].

Oxidation of disulfide bonds has been extensively studied under a variety of conditions [70-74], and Cu^{2+} promotes oxidative cleavage of disulfide bonds to form sulfinates [43,44]. Although O_2 is the oxidant in these reactions, Cu^{2+} plays a critical role in disulfide oxidation, as opposed to other transition metals such as Zn^{2+} [34]. Sulfur extrusion by oxidation is only observed for aromatic, heterocyclic thiones [29-33,42], giving support to the nucleophilic aromatic substitution mechanism in Scheme 5 as well as the importance of copper coordination to keep the nucleophilic thiolate in proximity to the site of nucleophilic attack.

This mechanism, including cycling of Cu^{2+} to Cu^{+} and back to Cu^{2+}, suggests future directions for design of sulfur extrusion catalysts, such as in desulfurization reactions for rubber recycling [75] as well as potential sulfur polymerization reactions for materials applications [76]. MMI performs two distinct roles that could be separated in a designed catalyst: (1) forming the disulfide species and (2) sulfur oxidation and subsequent extrusion. An aromatic imidazole thione, perhaps with electron-withdrawing substituents on the olefinic carbons, may be more resistant to oxidation by molecular oxygen and may therefore be more suitable for the first role. An analogous sulfur species where the sulfur is more amenable to oxidation (e.g., HMI) may function better in the sulfur extrusion role. A desymmetrized sulfur-extruded product would also likely be more amenable for subsequent C-S bond cleavage than the current symmetric bis(imidazole)thioether product, a process that would regenerate the thione in a catalytic cycle.

Additionally, neighboring group effects have been demonstrated to exert incredible rate acceleration/pH dependence in related systems [77]. In this context, a nucleophilic alcohol functional group (present either through replacement of the methyl substitution on the imidazole ring or from additional ligands on the metal center) could replace the initial nucleophilic attack by solvent, and then be liberated at a later step by a solvent, similar to the proteolytic mechanism of the catalytic triad in trypsin and other proteases [78].

4. Conclusions

Control of Cu^{+} and Cu^{2+} reactions with methimazole was explored utilizing a variety of counterions, solvents, and the presence or absence of oxygen. In the absence of oxygen, Cu^{+} reacts with MMI to form multinuclear complexes stabilized by bridging thiones and pi-stacking, indicating an environment rich in electrons. In the presence of oxygen with tetrafluoroborate counterion, the dinuclear $[Cu_2(MMI)_6][BF_4]_2$ complex is the favored product with both Cu^{+} and Cu^{2+} as the copper starting material. In the presence of oxygen and nitrate, sulfur extrusion by oxidation of the MMI^{DS} ligand results in the formation of a variety of Cu^{2+}-MMI^{MS} complexes, with variation introduced by the solvent system and molar ratios of ligand available. To form MMI^{MS}, oxidation and elimination of the sulfite or methylsulfite likely occurs to generate sulfate and methylsulfate ions, catalytically oxidized by the available copper. Cu^{2+} coordination likely imposes entropic control to align the newly formed thiolate group appropriately for nucleophilic aromatic substitution.

Previously published mechanistic descriptions were lacking in detail and did not explain the multiple products we obtained. This work provides new mechanistic insight into the reactivity of the imidazole thione, methimazole. Copper-promoted formation of a thiyl radical promotes

copper redox, sulfur oxidation, and nucleophilic attack. Ultimately, this reaction leads to sulfur extrusion by a nucleophilic aromatic substitution mechanism as well as formation of sulfate, methylsulfate, or hydrogensulfate counterions, depending on reaction conditions and solvent. Understanding this mechanism may lead to the design of novel catalysts for desulfurization reactions and synthesis of sulfur-containing polymers.

Abbreviations

DMPO – 2,2-dimethyl-3,4-dihydro-*2H*-pyrrole 1-oxide

EPR – electron paramagnetic resonance

ESI-HRMS – electrospray ionization high-resolution mass spectrometry

HMI – 2-mercaptoimidazole

MALDI-MS – matrix-assisted laser desorption ionization mass spectrometry

MMI – 2-mercapto-1-methylimidazole, methimazole

MMI^{DS} – bis(1-methylimidazol-2-yl)disulfide

MMI^{MS} – bis(1-methylimidazol-2-yl)sulfide

Appendix A. Supplementary data

Supplementary data associated with this article including crystallographic data for all structures; discussion of coordination polymers **10** and **11**; high-resolution mass spectrometry data for **4** and **9**; and additional EPR spectra can be found, in the online version, at https://. CCDC 1969547-1969557 contains the supplementary crystallographic data for this paper. These data can be obtained free of charge from The Cambridge Crystallographic Data Centre via www.ccdc.cam.ac.uk/structures.

Acknowledgments

We thank the National Science Foundation grant CHE 1213912 and 1807709 for support. J.M.M. thanks Clemson University Graduate School for a Doctoral Dissertation Completion Grant.

References

[1] E.S. Raper, Coord. Chem. Rev. 129 (1994) 91-156.

[2] T.S. Lobana, R. Sultana, G. Hundal, Polyhedron 27 (2008) 1008-1016.

[3] T. Suzuki, J. Matsumoto, Y. Kajita, T. Inomata, T. Ozawa, H. Masuda, Dalton Trans 44 (2015) 1017-1022.

[4] B.S. Stadelman, M.M. Kimani, C.A. Bayse, C.D. McMillen, J.L. Brumaghim, Dalton Trans 45 (2016) 4697-4711.

[5] W.-G. Jia, Y.B. Huang, Y.-J. Lin, G.-X. Jin, Dalton Trans. (2008) 5612-5620.

[6] H.R. Kim, I.G. Jung, K. Yoo, K. Jang, E.S. Lee, J. Yun, S.U. Son, Chem. Commun. 46 (2010) 758-760.

[7] L. Maria, C. Moura, A. Paulo, I.C. Santos, I. Santos, J. Organomet. Chem. 691 (2006) 4773-4778.

[8] Y. Peng, L. Shang, Y. Cao, G.I. Waterhouse, C. Zhou, T. Bian, L.Z. Wu, C.H. Tung, T. Zhang, Chem. Commun. 51 (2015) 12556-12559.

[9] Y.-C. Pan, Y. Wen, L.-Y. Xue, X.-Y. Guo, H.-F. Yang, J. Phys. Chem. C 116 (2013) 3532-3538.

[10] B.G. Ateya, B.E. El-Anadouli, F.M.A. El-Nizamy, Bull. Chem. Soc. Jpn. 54 (1981) 3157-3161.

[11] N. O'Connor, G.E. Lopez, A. Cruz, Curr. Chem. Lett. 3 (2014) 189-194.

[12] G.Y. Roy, P.N. Jayaram, G. Mugesh, Chem. Asian. J. 8 (2013) 1910-1921.

[13] G. Parkin, New J. Chem. 31 (2007) 1996-2014.

[14] M.M. Kimani, C.A. Bayse, J.L. Brumaghim, Dalton Trans. 40 (2011) 3711-3723.

[15] E.W. Ainscough, A.M. Brodie, Coord. Chem. Rev. 27 (1978) 59-86.

[16] I. Kravets, Am. Fam. Physician 93 (2016) 363-370.

[17] D. Manna, G. Roy, G. Mugesh, Acc. Chem. Res. 46 (2013) 2706-2715.

[18] I.K. Cheah, R.M. Tang, T.S. Yew, K.H. Lim, B. Halliwell, Antioxid. Redox Signal. 26 (2017) 193-206.

[19] E.R. Atkinson, A.R. Jackson, E.S. Raper, Inorg. Chim. Acta 92 (1985) 35-41.

[20] P.A. Karagiannidis, P. Aslanidis, S. Papastefeanou, D. Mentzafos, A. Hountas, A. Terzis, Polyhedron 9 (1990) 981-986.

[21] J.R. Creighton, A.C. Gorvin, C. Getteridge, A.R. Jackson, E.S. Raper, P.M. Sherwood, Inorg. Chim. Acta 103 (1985) 195-205.

[22] E.S. Raper, W. Clegg, Inorg. Chim. Acta 180 (1991) 239-244.

[23] E.S. Raper, D. Robson, J.D. Wilson, W. Glegg, A. Milne, Inorg. Chim. Acta 1432 (1988) 98-100.

[24] E.R. Atkinson, E.S. Raper, D.J. Gardiner, H.M. Dawes, N.P. Walker, A.R. Jackson, Inorg. Chim. Acta 100 (1985) 285-291.

[25] E.S. Raper, J.R. Creighton, W. Clegg, Inorg. Chim. Acta 183 (1991) 179-187.

[26] E.S. Raper, J.R. Creighton, J.D. Wilson, W. Clegg, A. Milne, Inorg. Chim. Acta 155 (1989) 77-83.

[27] T.S. Lobana, R. Sultana, G. Hundal, R.J. Butcher, Polyhedron 28 (2009) 1573-1577.

[28] J.J. Warren, K.M. Lancaster, J.H. Richards, H.B. Gray, J. Inorg. Biochem. 115 (2012) 119-126.

[29] T.S. Lobana, R. Sultana, R.J. Butcher, A. Casieneiras, T. Akitsu, F.J. Fernandez, M.C. Vega, Eur. J. Inorg. Chem. 2013 (2013) 5161-5170.

[30] E.W. Ainscough, A.M. Brodie, G.J. Gainsford, Inorg. Chim. Acta 180 (1991) 81-83.

[31] E.W. Ainscough, B.F. Anderson, E.N. Baker, A.G. Bingham, A.M. Brodie, Inorg. Chim. Acta 105 (1985) L5-L7.

[32] D.A. Baldwin, L. Denner, A.J. Marwell, J. Crystallogr. Spectrosc. Res. 14 (1984) 157-167.

[33] D.A. Baldwin, L. Denner, A.J. Markwell, J. Crystallogr. Spectrosc. Res. 16 (1986) 763-768.

[34] K.K. Kimura, I. Kinoshit, N. Nakashima, K. Kitano, T. Nichioka, K. Isobe, Chem. Commun. (1999) 497-498.

[35] C.L. Merrill, L.J. Wilson, T.J. Thaamann, J. Thomas, T.M. Loehr, N.S. Ferris, W.H. Woodruff, J. Chem. Soc., Dalton Trans. 10 (1984) 2207-2221.

[36] E.L. Que, E. Gianolio, S.L. Baker, S. Aime, C.J. Chang, Dalton Trans (2010) 469-476.

[37] Bruker Axis, Inc., Madison, WI, 2015.

[38] G. Sheldrick, Acta Crystallogr. A 64 (2008) 112-122.

[39] A. Spek, Acta Crystallogr. Sec.t C Struct. Chem. 71 (2015) 9-18.

[40] S. Stoll, A. Schweiger, J. Magn. Reson. 178 (2006) 42-55.

[41] D.R. Duling, J. Magn. Reson. 104 (1994) 105-110.

[42] T.S. Lobana, R. Sultrana, G. Hundal, R.J. Butcher, Dalton Trans. 39 (2010) 7870-7872.

[43] A. Odani, T. Maruyama, O. Yamauchi, T. Fujiwara, K. Tomita, J. Chem. Soc., Chem. Commun. (1982) 646-647.

[44] L.S. Higashi, M. Lundeen, E. Hilti, K. Seff, Inorg. Chem. 16 (1977) 310-313.

[45] O. Yamauchi, A. Odani, Pure Appl. Chem. 68 (1996) 469-496.

[46] V. Aggarwal, V. Ram Kumar, U.P. Signh, J. Chem. Cryst. 41 (2011) 121-1126.

[47] J.S. Figueroa, K. Yurkerwich, J. Melnick, D. Buccella, G. Parkin, Inorg. Chem. 46 (2007) 9234-9244.

[48] Y. Matsunaga, K. Fujisawa, N. Amir, Y. Miyashita, K. Okamoto, Appl. Organomet. Chem. 19 (2005) 208.

[49] R. Rajasekharan-Nair, A. Marckwordt, S.T. Lutta, M. Schwalbe, A. Biernat, D.R. Armstrong, A.J. Watson, A.R. Kennedy, J. Reglinski, M.D. Spicer, Chemistry 19 (2013) 13561-13568.

[50] G. Vampa, S. Benvenuti, F. Severi, L. Malmusi, L. Antolini, J. Heterocycl. Chem. 32 (1995) 227-234.

[51] G.B. Ansell, J.Chem. Soc., Perkin Trans. 2 (1972-1999) (1972) 841-843.

[52] M. Trost, W.L. Schinski, F. Chen, I.B. Mantz, J. Am. Chem. Soc. 93 (1971) 676-684.

[53] E.J. Corey, A.E. Winter, J. Am. Chem. Soc. 85 (1963) 2677-2678.

[54] J.Q. Chambers, P.R. Moses, R.N. Shelton, J. Electroanal. Chem. (1972) 245-248.

[55] J. Peisach, W.E.Blumberg, Arch. Biochem. Biophys. 165 (1974) 691-708.

[56] E. Garribba, G. Micera, J. Chem. Educ. 83 (2006) 1229-1232.

[57] S.K. Hoffmann, J. Goslar, S. Lijewski, A. Zalewska, J. Magn. Reson. 236 (2013) 7-14.

[58] G.R. Buettner, Free Radic. Res. Commun. 19 (1993) S79-S87.

[59] L.S. Harman, C. Mottley, R.P. Mason, J. Biol. Chem. 259 (1984) 5606-5611.

[60] L. Graf, S. Fallab, Experientia 20 (1964) 46-47.

[61] H.J. Hartmann, C. Sieves, U. Weser, Radicals in biochemically important thiols in the presence of metal ions, in: Metal ions in biological systems, 1999, pp 389-413.

[62] D. Deter, H.J. Hartmann, U. Weser, Biochem. Biophys. Acta 78 (1994) 344-347.

[63] M. Younes, U. Weser, Biochem. Biophys. Res. Commun. 78 (1977) 1247-1253.

[64] F.A. Villamena, J.K. Merle, C.M. Hadad, J.L. Zweier, J. Phys. Chem. A 109 (2005) 6089-6098.

[65] H. Zhao, J. Joseph, H. Zhang, H. Karoui, B. Kalyanaraman, Free Rad. Bio. Med. 31 (2001) 599-606.

[66] R.K. Rai, A. Chalana, R. Karri, R. Das, B. Kumar, G. Roy, Inorg. Chem. 58 (2019) 6628-6638.

[67] E. Abel, Monatsh. Chem. 82 (1951) 815-834.

[68] C. Brandt, R. van Eldik, Chem. Rev. 95 (1995) 119-190.

[69] T. Kan, T. Fukuyama, Chem. Commun. (2004) 353.

[70] P. Natarajan, Tetrahedron Lett. 56 (2015) 4131-4134.

[71] T. Wandini, Y. Einaga, Chem. Sens. 21 (2005) 10-12.

[72] T. Mukawa, T. Goto, T. Takeuchi, Analyst 127 (2002) 1407-1409.

[73] J.L. Kice, A.R. Puls, J. Am. Chem. Soc. 99 (1977) 3455-3460.

[74] J.A. Maclaren, S.J. Leach, I.J. O'Donnell, Biochim. Biophys. Acta 35 (1959) 280-281.

[75] R.A. Sanchez-Delgado, J. Mol. Catal. 86 (1994) 287-307.

[76] W.J. Chung, J.J. Griebel, E.T. Kim, H. Yoon, A.G. Simmonds, H.J. Ji, P.T. Dirlam, R.S. Glass, J.J. Wie, N.A. Nguyen, B.W. Guralnick, J. Park, A. Somogyi, P. Theato, M.E. Mackay, Y-E.Sung, K. Char, J. Pyun, Nat. Chem. 5 (2013) 518-524.

[77] A. Wagenaar, A.J. Kirby, B.F.N. Jan, Tetrahedron Lett. 43 (1974) 3735-3738.

[78] G. Dodson, A. Wiodawer, Trends Biochem. Sci. 23 (1998) 347-352.